Available online at www.sciencedirect.com
ScienceDirect
Trans. Nonferrous Met. Soc. China 34(2024) 2007−2019
Transactions of Nonferrous Metals Society of China
www.tnmsc.cn

Separation of fluorine and aluminum from secondary aluminum dross by calcium-cured alkali roasting−water leaching

Liang-min DONG[1,2], Fen JIAO[1,2], Wei LIU[1,2], Ya-lin HUANG[1,2], Xin WEI[1,2], Wen-qing QIN[1,2]

1. School of Minerals Processing and Bioengineering, Central South University, Changsha 410083, China;
2. Key Laboratory of Hunan Province for Clean and Efficient Utilization of Strategic Calcium-containing Mineral Resources, Central South University, Changsha 410083, China

Received 12 January 2023; accepted 11 October 2023

Abstract: A combined strategy of calcium-cured alkali roasting and water leaching was devised to treat secondary aluminum dross. The effects of calcium oxide dosage, sodium hydroxide dosage, roasting temperature, and time on aluminum extraction behavior and fluorine curing behavior were studied. Under optimal experimental conditions: roasting temperature of 1000 °C, Al∶NaOH mole ratio of 1∶0.6, F∶CaO mole ratio of 1∶2.5, and roasting time of 2.0 h, fluorine and aluminum were separated, with 99.98% of the fluoride solidified and 52.97% of the aluminum extracted. The sodium aluminate products obtained by evaporation and crystallization from leaching solution met the industrial standards of China. The aqueous residue can be used as a raw material for quick-setting cement. Overall, this study provides an effective and environmentally friendly strategy for the treatment of secondary aluminum dross.

Key words: secondary aluminum dross; calcium-cured alkali roasting; separation; fluorine; aluminum; sodium aluminate; clean production

1 Introduction

Aluminum is the world's largest non-ferrous metal in terms of generation and utilization [1]. Molten salt electrolysis is the currently most successful treatment of aluminum production [2]. A considerable amount of solid hazardous waste in molten salt electrolysis is a serious issue. In particular, aluminum dross is one of the intractable problems that must be urgently addressed [3,4]. Aluminum dross contains a variety of toxic substances namely, aluminum nitride (AlN), aluminum carbide (Al_4C_3), soluble fluoride (NaF, KF), and chlorine salts (NaCl, KCl) [5,6]. The generation of aluminum is usually accompanied with the formation of extensive aluminum dross. About 1 t of aluminum can produce 10−15 kg of aluminum dross [7]. The electrolytic aluminum industry produced 65.27×10^6 t of primary aluminum in 2020, and the aluminum dross yield exceeded 652×10^3 t [8]. With the continuous strictness of natural prerequisites and the development of resource reuse, aluminum dross needs to be disposed properly. Landfilling is the foremost broadly utilized strategy for the disposal of aluminum dross [9,10]. However, burying of dross occupies precious land and leads to potential environmental threat. Meanwhile, aluminum dross contains numerous profitable components and is a recoverable secondary resource [11].

In recent years, various pyrometallurgical and

Corresponding author: Fen JIAO, Tel: +86-13549683403, E-mail: jfen0601@126.com;
Wei LIU, Tel: +86-13787007421, E-mail: liuweipp1@126.com
DOI: 10.1016/S1003-6326(24)66522-2

hydrometallurgical processes have been established for the reuse of aluminum dross. With regard to the pyrometallurgical processes, the most prevalent processes are the salt bath and salt-free strategy. The salt bath process mainly consists of the fried dross method [12,13] and the tilting rotary kiln method [14,15], in which aluminum metal is liquefied over 700 °C in the presence of a complex salt and ends up separating [16]. The salt-free processes incorporate press [17], plasma quick-melt [18], and centrifugal separation [19]. During salt-free processes, high temperature directly destroys the oxide layer on the surface of aluminum droplets, and nearly 90% of the aluminum metal can be recuperated [15]. However, the direct recycling of aluminum metal is a complex process with high vitality utilization [20].

Hydrometallurgy can recover a variety of profitable components from aluminum dross. The most common wet disposal strategies are acid leaching [21−23], and alkaline leaching [24−26]. Acid leaching recuperates profitable components, and most metal oxides are decomposed, which creates difficulties in the subsequent product purification and leads to a large amount of waste liquid that cannot be recovered. By contrast, alkali leaching can ensure the purity of the leachate, shorten the process, and reuse the leachate. However, alkali leaching alone is unable to reclaim productively the valuable materials efficiently. Aluminum dross also has been developed for the preparation of materials such as spinel, mullite, and cryolite, as well as for the preparation of water purifiers [27−31]. Although different treatments of converting aluminum dross have met the industrial manufacture demands, they are unsuitable for daily application due to some deficiencies. For example, aluminum dross cannot be applied to a water purifier because of the inevitable combination between aluminum and fluoride, which is difficult to remove [32]. The chemical composition of aluminum dross is closely related to the raw materials, operating conditions, and generation forms of the aluminum process [33,34]. Consequently, a cost-effective and environment-friendly innovation must urgently be created to reuse the profitable assets from aluminum dross.

In this work, a combination of calcium-cured alkali roasting and water leaching was innovatively proposed for the disposal of aluminum dross. Compared with the traditional harmless roasting process, our new method has economic and ecological advantages because it incorporates the resourceful recycling of waste. the effects of NaOH dosage, CaO dosage, roasting temperature, and time on the aluminum extraction and fluorine solidification behavior were systematically investigated. The quality of the $NaAlO_2$ products obtained by evaporation, concentration, and crystallization of the leachate was examined. During the whole study, phase evolution and surface morphology were analyzed by X-ray powder diffraction (XRD) and scanning electron microscopy associated with energy- dispersive spectroscopy (SEM-EDS).

2 Experimental

2.1 Materials and analysis

The secondary aluminum dross utilized in the study was obtained from an electrolytic aluminum plant in Inward Mongolia, China, and the dross was generated from the slagging process. First, the raw material was washed before roasting. The purpose of washing to remove chlorine salts (99.89%) and soluble fluoride (99.93%) is to ensure the purity of the consequent products. Under the optimal conditions: leaching temperature of 95 °C, leaching time of 11.2 h, and liquid-to-solid ratio of 7.8∶1 (mL/g), the recovery of AlN reached 92.49% and the product was prepared as $(NH_4)_2SO_4$. Prior to the experiments, the washed material was dried at (100±5) °C in a draught drying cabinet and blended completely. Representative samples were obtained by coning and quartering strategies for experiments. A portion of the sample was ground to be less than 74 μm to prepare specimens for examination. The main chemical composition of the dross is shown in Table 1. The contents (mass fraction) of Al, F, Na, K, and Ca in washed slag were 39.76%, 11.00%, 6.60%, 2.25%, and 0.82%, respectively. The results of XRD and SEM−EDS analyses for the washed slag are shown in Fig. 1. Figure 1(a) indicates that the main components were corundum (α-Al_2O_3), cryolite (Na_3AlF_6), calcium fluoride (CaF_2), and boehmite (y-AlOOH), with y-AlOOH being delivered by the washing treatment [35]. Figure 1(b) shows that the samples had complex components, different shapes, and different particle sizes, and they were wrapped with one another. The large

Table 1 Main chemical composition of washed aluminum dross (wt.%)

Al	F	Na	K	Ca	Si	Fe	Mg
39.76	11.00	6.60	2.25	0.82	0.68	0.21	0.09

particle was mainly composed of Al and O, existing in the form of Al_2O_3; the fine white particles were a tight combination of Na, Al, F, O, Si, Ca, and Mg.

All reagents utilized for the experiment and chemical analysis were of analytical grade. Sodium hydroxide (NaOH) and calcium oxide (CaO) were used for calcium-cured alkali roasting, trisodium citrate ($C_6H_5Na_3O_7$) was used for buffer preparation, nitric acid (HNO_3) was used for pH alteration, and thymol blue ($C_{27}H_{30}O_5S$) was used as an indicator. Deionized water with a resistivity of 18 MΩ·cm was used throughout all analyses, and it was prepared through a laboratory water purification system (Medium−1600). Meanwhile, the main equipments used in the test were a muffle furnace, water bath, electronic scales, and other equipment.

2.2 Experimental setup and procedure

The calcium-cured alkali roasting experiments were performed in a muffle furnace (KJ, GSL-1700X-III). For each test, 50.0 g of the prepared washing aluminum dross was completely blended with NaOH and CaO at a planned proportion. The mixed samples were stacked in a ceramic crucible (200.0 mL) and fixed with a cover. The ceramic crucible was placed into the thermostatic heating zone of the muffle furnace. Subsequently, the temperature of this mixed sample was raised at a rate of 10 °C/min until the time set by the program when it reached the required temperature. The furnace was cooled to laboratory temperature when the process was completed. Finally, the roasted sample was removed, collected, weighed, and sieved for subsequent examination and experiments.

The water leaching experiments were conducted in a 300.0 mL glass conical flask, which was equipped with a mechanical stirrer, temperature controller, and water bath. Before the experiments, $C_6H_5Na_3O_7$, NaOH, HNO_3, and $C_{27}H_{30}O_5S$ solutions were prepared at the concentrations required to determine the fluoride ions in the solution. 20.0 g of the roasting sample was then weighed and placed in a warmed conical flask with the liquid-to-solid ratio

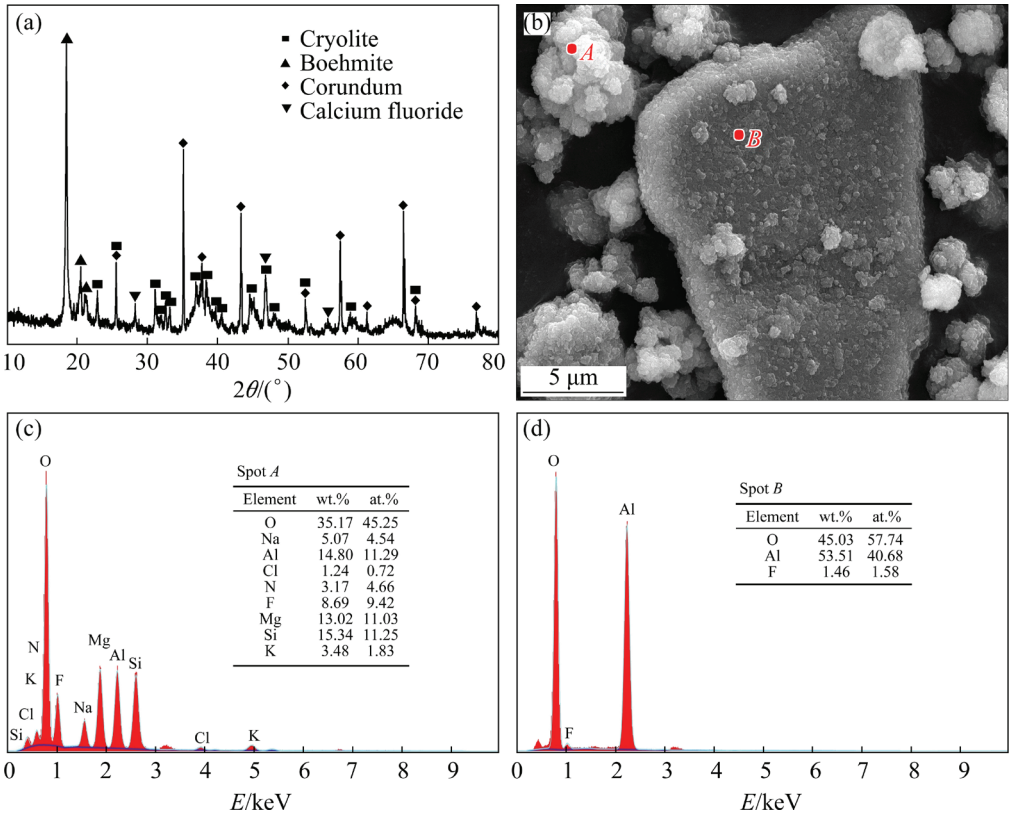

Fig. 1 XRD pattern (a), SEM image (b), and corresponding EDS analysis (c, d) of washed aluminum dross

and temperature adjusted for leaching. At the end of each leaching experiment, the slurry was filtered by a vacuum filter. The volume of leachate was measured, the concentration of aluminum was analyzed by ICP-AES, the concentration of fluorine was analyzed by fluoride ion counter, and the solid product was obtained by evaporation crystallization. The residues and products were dried, weighed, and analyzed by XRD, SEM−EDS, and chemical element analyses.

In this study, the leaching rate of aluminum and the degree of fluorine curing were important indexes to evaluate the effectiveness of calcium curing alkali roasting, which were calculated by Eqs. (1) and (2), respectively. Previous studies have found that the boiling point for fluoride volatilization at atmospheric pressure is above 1000 °C, which implies that fluoride volatilization could not occur in this experiment [36,37]. Therefore, the aluminum dissolution rate and the fluorine curing rate were calculated by the following formulas:

$$\varepsilon=\frac{c_1 V n_1 m_1}{20 m y_1}\times 100\% \quad (1)$$

$$\theta=(1-\frac{c_2 v n_2 m_1}{20 m_2 y_2})\times 100\% \quad (2)$$

where ε and θ are the aluminum dissolution rate and the fluorine curing rate, respectively; c_1 and c_2 are the aluminum and fluorine concentrations tested, respectively; m_1 and m_2 are the mass of roasted samples and waterlogged samples, respectively; V is the volume of water submersion fluid; n_1 an n_2 are the dilution multiples for aluminum and fluorine tests in the water leach solution, respectively; y_1 and y_2 are the total aluminum and fluorine contents in the roasted sample, respectively.

The primary guideline of the fluorine content test is that the concentration of fluorine influences the changes in the electromotive force of the battery, which follows the Nernst equation. When the total ionic strength is high, the following relationship is obeyed:

$$\varphi=\varphi^{\ominus}-\frac{2.303RT}{F}\cdot\lg F_1 \quad (3)$$

where φ is the electrode potential, $\varphi^{\ominus}$ is the standard electrode potential, R is the molar gas constant, T is the temperature, F is Faraday's constant, and F_1 is the fluoride ion concentration of the solution to be measured.

The working battery can be expressed as Ag|AgCl , Cl^- (0.300 mol/L), F^- (0.001 mol/L) |LaF_3| |Test solution| |External reference electrode|.

2.3 Analytical methods

The aluminum contents of raw materials and all leached slags were detected by inductively coupled plasma-atomic emission spectrometry (ICP-AES, IRIS Intrepid II XSP). The contents of fluorine in raw materials and all leached slags were determined by chemical analysis methods (HJ 999-2018) and the elemental fluorine was detected by fluoride ion counter (PXSJ−216F, INESA) according with the GB/T 21057−2007. The crystallographic compositions of raw material, roasted slags and leached slags were characterized by X-ray powder diffraction (XRD, Germany Bruker-axsD8 Advance), operating at 40 kV and 20 mA, varying from 10° to 80° at scanning rate of 10 (°)/min. The morphological characteristics and elements distribution of the raw material, slags and products were identified by a scanning electron microscopy (SEM, JEOL, JSM6490LV) associated with energy-dispersive spectroscopy (EDS, JEOLJSM−6490LV) analysis.

3 Results and discussion

3.1 Thermodynamic analysis

According to the chemical analysis results, the aluminum dross was rich in aluminum and fluorine. Aluminum is primarily found in Al, α-Al_2O_3, Na_3AlF_6, and AlN, whereas; fluorine is found in Na_3AlF_6 and CaF_2. Previous studies have reported that aluminum could be converted to $NaAlO_2$ and fluorine to CaF_2 and $Ca_{12}Al_{14}F_2O_{32}$ with the increase of roasting temperature [38,39]. Consequently, the reactions that occurred during calcium-cured alkali roasting were as follows:

$$2Al+2NaOH+2H_2O=2NaAlO_2+3H_2\uparrow \quad (4)$$

$$Al_2O_3+2NaOH=2NaAlO_2+H_2O \quad (5)$$

$$AlN+NaOH+H_2O=NaAlO_2+NH_3\uparrow \quad (6)$$

$$17CaO+6Al_2O_3+2Na_3AlF_6=5CaF_2+3Na_2O+Ca_{12}Al_{14}F_2O_{32} \quad (7)$$

$$36CaO+Na_3AlF_6+22Al_2O_3=3NaAlO_2+3Ca_{12}Al_{14}F_2O_{32} \quad (8)$$

$$CaF_2+2NaOH=2NaF+Ca(OH)_2 \quad (9)$$

$$11CaO+7Al_2O_3+CaF_2=Ca_{12}Al_{14}F_2O_{32} \quad (10)$$

The Gibbs free energy changes (ΔG) for these reactions from 100 to 1100 °C were calculated by the Reaction module with FactSage 8.0. Figure 2 displays that ΔG for all reactions was less than zero at 100−1100 °C, demonstrating that all reactions could theoretically occur. With the increase in temperature, ΔG of Eqs. (5), (7) and (8) decreased, indicating that increasing temperature favored these reactions. Equations (4), (6) and (9) show that ΔG increased with increasing temperature. It showed that, increasing temperature retards the reaction of NaOH with Al, AlN, and CaF_2, further showing that increasing temperatures reduced the conversion of CaF_2 to NaF. Above 400 °C, ΔG for Eq. (9) was greater than that for all other reactions, so the reaction was only possible under excess NaOH. Thus, excess NaOH led to the conversion of CaF_2 to NaF. The results showed that the use of NaOH as a modifier for aluminum and CaO as a fixing agent for fluorine was thermo- dynamically feasible.

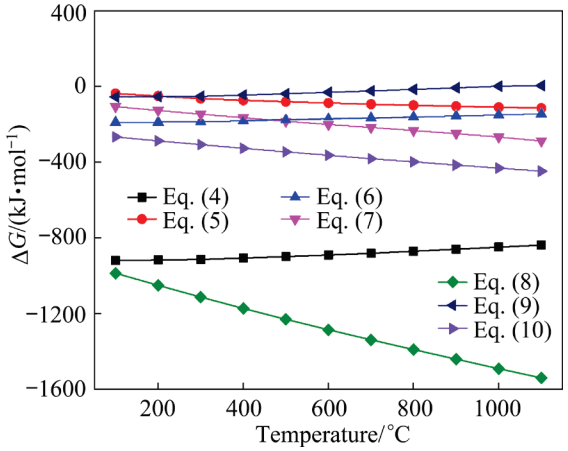

Fig. 2 ΔG of possible reactions as function of temperature

Meanwhile, the total fluorine content was calculated to be no more than 20% according to Eqs. (7) and (8). Figure 3 shows the ternary phase diagram calculated using the phase diagram module in FactSage 8.0, which was centered on the heading of the component fluorine. As shown in Fig. 3(a), fluoride was only present in the form of CaF_2 when the content of Al_2O_3 was between 0 and 12%. The fluoride transformed into a mixture of CaF_2 and $Ca_{12}Al_{14}F_2O_{32}$, when the amount of Al_2O_3 reached 12%−62%. The reaction of Na_3AlF_6 in not complete when Al_2O_3 is 90%. The continuing reaction was impeded as the content of Al_2O_3 continued to increase to 100%. Meanwhile, the increasing temperature had no effect on the phase change transformation of fluoride. Compared with Fig. 3(a), increasing the amount of Na_3AlF_6 revealed a highly complex fluoride orientation. According to Fig. 3(b), as the phase of CaF_2 increased, the phase co-existing as CaF_2 and $Ca_{12}Al_{14}F_2O_{32}$ diminished, and the unreacted phase increased. Thus, the amount of CaO must be centered to guarantee that fluoride could be completely cured.

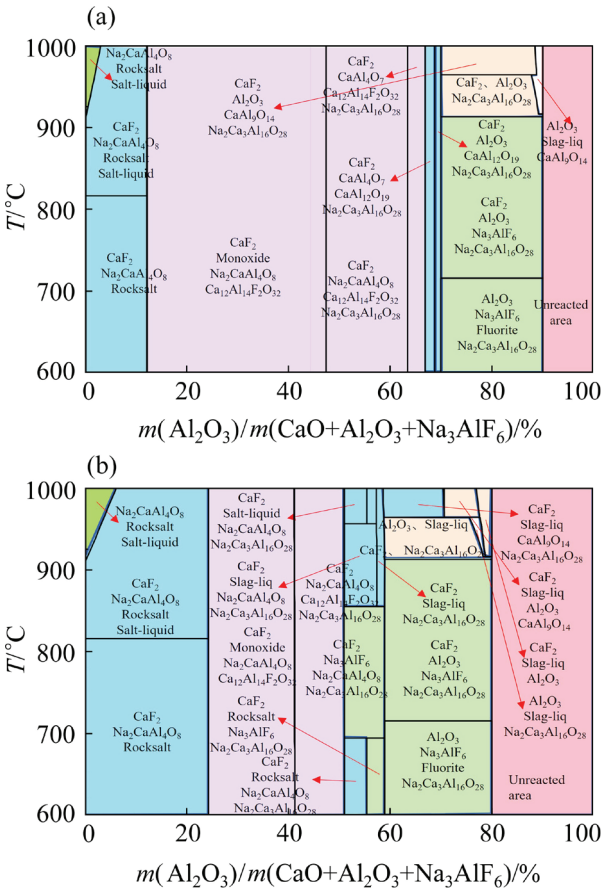

Fig. 3 Phase diagram of Na_3AlF_6−Al_2O_3−CaO system under 0.1 MPa: (a) $w(Na_3AlF_6)$=10%; (b) $w(Na_3AlF_6)$=20%

3.2 Effects of calcium-cured alkali roasting conditions

In this work, the calcium-cured alkali roasting of aluminum dross was studied by thermodynamic analysis, and some positive results were obtained. A series of experiments should be carried out to further investigate the dissolution rate of aluminum and solidification rate of fluorine. The effects of experimental conditions such as CaO dosage,

NaOH dosage, roasting temperature, and time on aluminum dissolution rate and fluorine curing rate in aluminum dross were examined, and the results are presented in Fig. 4.

In theoretical calculations, CaO dosage plays a critical role during calcium-cured alkali roasting (Eqs. (7) and (8)). Therefore, the effect of different of F to CaO mole ratios on the solidification rate of fluoride and the dissolution rate of aluminum at 1000 °C, a Al to NaOH mole ratio of 1:0.6, and a roasting time of 2.0 h was investigated. Figure 4(a) shows that the solidification rate of fluorine increased when the mole ratio of F to CaO increased from 1:1.0 to 1:2.5. However, as the mole ratio of F to CaO reached 1:3.5, the solidification rate of fluorine stayed the same at 99.98%. This result could be attributed to the fact that the increment of CaO promoted the conversion of fluoride to stable material CaF_2 and $Ca_{12}Al_{14}F_2O_{32}$ (Eqs. (7) and (8)). In addition, the leaching rate of aluminum showed no shift with increasing mole ratio of F to CaO, and it remained at 52.97%. The aluminum compounds that were generated with the involvement of CaO could not be broken down within the watery arrangement. This result showed that the amount of CaO had a remarkable influence on the curing rate of fluorine but only slightly affected the leaching rate of aluminum. Considering the steady curing of fluoride and the economic effect, the optimum CaO dosage was F to CaO mole ratio of 1:2.5. Other tests were performed on this premise.

Thermodynamic calculations revealed that different amounts of NaOH could respond in various ways with aluminum and fluorine compounds at high temperatures (Eqs. (4)−(6) and (9)). Therefore, the effect of NaOH dosage on the solidification rate of fluorine and the dissolution rate of aluminum was investigated at 1000 °C, F to CaO mole ratio of 1:2.5, and roasting time of 2.0 h. In Fig. 4(b), as the mole ratio of Al to NaOH increased from 1:0.6 to 1:1.4, the solidification rate of fluorine diminished from 99.98% to 60.52% and the dissolution rate of aluminum increased from 52.97% to 90.62%. With the increasing amount of NaOH, the reaction between aluminum compound and NaOH continued and produced more water-soluble substances (Eqs. (4)−(6) and (9)), which led to an increase in the dissolution rate of aluminum. Simultaneously, the soluble products conjointly

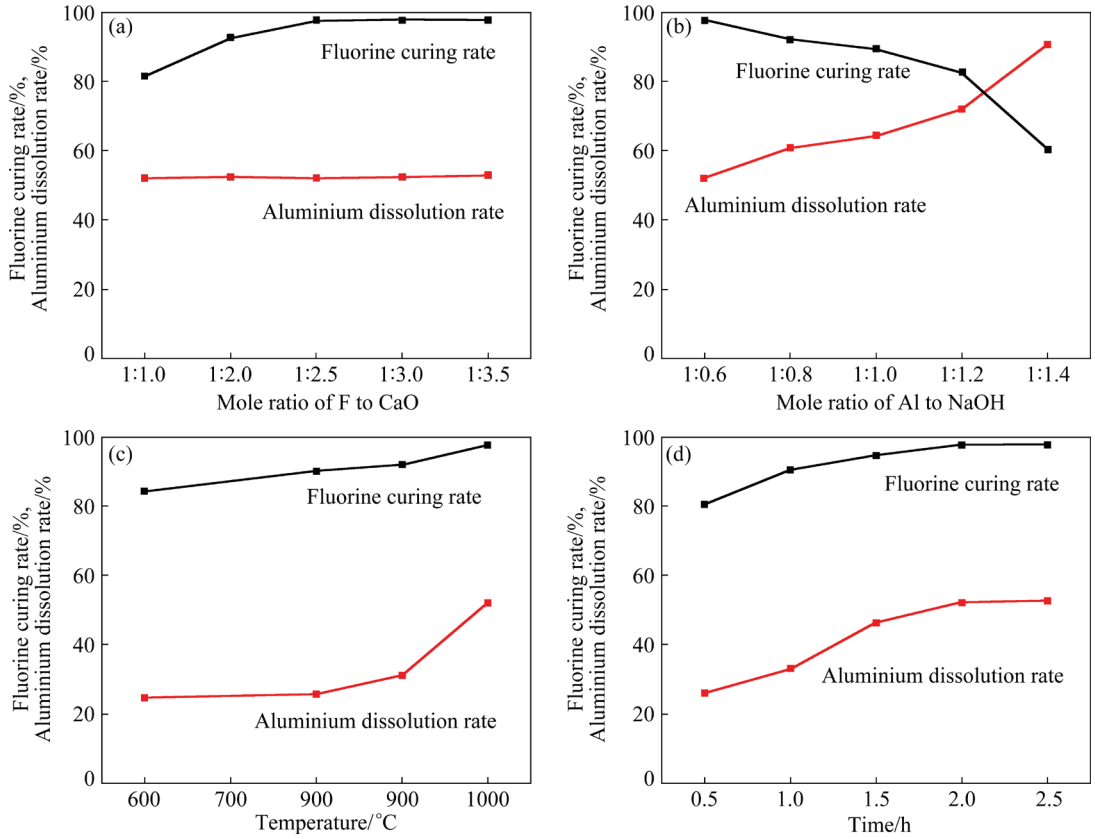

Fig. 4 Fluorine curing rate and aluminum dissolution rate under different conditions: (a) Mole ratio of F to CaO; (b) Mole ratio of Al to NaOH; (c) Temperature; (d) Time

responded with the resulting $Ca_{12}Al_{14}F_2O_{32}$ in aqueous solution, leading to the dissolution of $Ca_{12}Al_{14}F_2O_{32}$ and a decrease in the rate of fluorine fixation (Eq. (11)).

$$Ca_{12}Al_{14}O_{32}F_2+16NaOH+4H_2O= 2NaF+14NaAlO_2+12Ca(OH)_2 \quad (11)$$

As shown in Table 2, ΔG of $Ca_{12}Al_{14}F_2O_{32}$ in alkaline solution was negative in the range of 10−90 °C, indicating that the reaction could proceed in the positive course. Therefore, an Al:NaOH mole ratio of 1:0.6 was chosen as the optimum NaOH dosage for this experiment to ensure an effective fluoride fixation rate.

The solidification rate of fluorine and the dissolution rate of aluminum were investigated at different roasting temperatures with Al to NaOH mole ratio of 1:0.6, F to CaO mole ratio of 1:2.5, and roasting time of 2.0 h. As shown in Fig. 4(c), as the temperature increased from 600 to 1000 °C, the curing rate of fluorine increased from 84.34% to 99.98% and the dissolution rate of aluminum increased from 24.82% to 52.97%. Meanwhile, the solidification rate of fluorine and the dissolution rate of aluminum were examined at different roasting time and a roasting temperature of 1000 °C, an Al:NaOH mole ratio of 1:0.6, and an F:CaO mole ratio of 1:2.5. As shown in Fig. 4(d), the solidification rate of fluorine and the dissolution rate of aluminum increased with the extension of the roasting time. In conclusion, the increased temperature and long roasting time favored the steady solidification of fluoride and the effective dissolution of the aluminum compounds. However, in the experiments, we observed a significant bonding of the roasted material until the roasting temperature reached 1100 °C. This step was carried out to ensure that the roasted material could be fed directly into the water leaching system without crushing and grinding in the subsequent stages. To prevent fluoride volatilization into the flue gas, we selected the optimum roasting temperature and time of 1000 °C and 2.0 h, respectively.

Table 2 ΔG of $Ca_{12}Al_{14}O_{32}F_2$ in alkaline solutions at different temperatures

Temperature/°C	ΔG/(kJ·mol^{-1})
10	−683.7
20	−681.0
30	−678.2
40	−675.4
50	−672.6
60	−669.7
70	−666.8
80	−663.8
90	−660.9

Figure 5 shows the mechanism of calcined alkali roasting−water leaching, which can effectively solidify fluoride and dissolve aluminum compounds in aluminum dross. The optimized conditions were as follows: roasting temperature of 1000 °C, Al to NaOH mole ratio of 1:0.6, F to CaO mole ratio of 1:2.5, and roasting time of 2.0 h. Under these conditions, the curing rate of fluorine was 99.98% and the dissolution rate of aluminum was 52.97%.

3.3 Phase transformations

The roasted samples were subjected to XRD analysis to further investigate the phase transformation behaviors of aluminum dross during

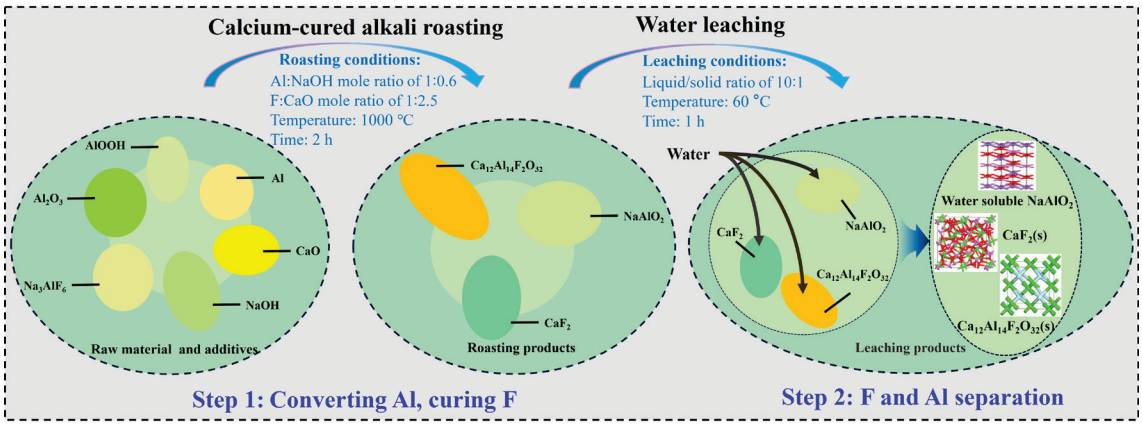

Fig. 5 Mechanistic diagram of calcined alkali roasting− water leaching

calcium-cured alkali roasting. Figure 6(a) shows the XRD patterns of the roasted samples at the same temperature, time and NaOH dosage, with diverse CaO dosages. The diffraction peak of Na_3AlF_6 slowly vanished and the intensity of the diffraction peak of $Ca_{12}Al_{14}F_2O_{32}$ gradually expanded with the increase of CaO dosage. When the CaO dosage reached the F to CaO mole ratio of 1:2.5, the diffraction peak of $Ca_{12}Al_{14}F_2O_{32}$ exhibited the most obvious trend. This result demonstrated the possibility of Eqs. (7) and (8) going forward with the increase in CaO dosage. Meanwhile, the increase in CaO dosage led to the decrease in the intensity of the diffraction peak of CaF_2, which may be due to the conversion of CaF_2 to $Ca_{12}Al_{14}F_2O_{32}$ (Eq. (10)). Thus, increasing the amount of CaO could effectively promote the stable curing of fluoride. Figure 6(b) shows the XRD patterns of the samples roasted at the same temperature, time, and CaO dosage but different NaOH dosages. The increase in the sum of NaOH significantly promoted the formation of $NaAlO_2$ and the disappearance of CaF_2 and $Ca_{12}Al_{14}F_2O_{32}$. Equations (9) and (10) occurred when the amount of NaOH increased. Therefore, the amount of NaOH should be strictly controlled in the experiment; otherwise, the effect of fluorine fixation may not be easily achieved.

Figure 6(c) shows the change in phase composition of the roasted sample at different temperatures. With increasing temperature, the intensity of the diffraction peaks of Al_2O_3, Al, and CaO slowly diminished, whereas the intensity of the diffraction peaks of CaF_2, $Ca_{12}Al_{14}F_2O_{32}$, and $NaAlO_2$ gradually increased. Equations (4), (5), (7) and (8) were promoted in the positive direction with increasing temperature, suggesting that increasing temperature favored the conversion of aluminum to $NaAlO_2$ and the solidification of fluorine to CaF_2 and $Ca_{12}Al_{14}F_2O_{32}$. Figure 6(d) shows the change in phase composition of the roasted sample at different time. The diffraction peaks of $Ca_{12}Al_{14}F_2O_{32}$, CaF_2, and $NaAlO_2$ continuously increased and intensified as time increased. When the time reached 2.0 h, the

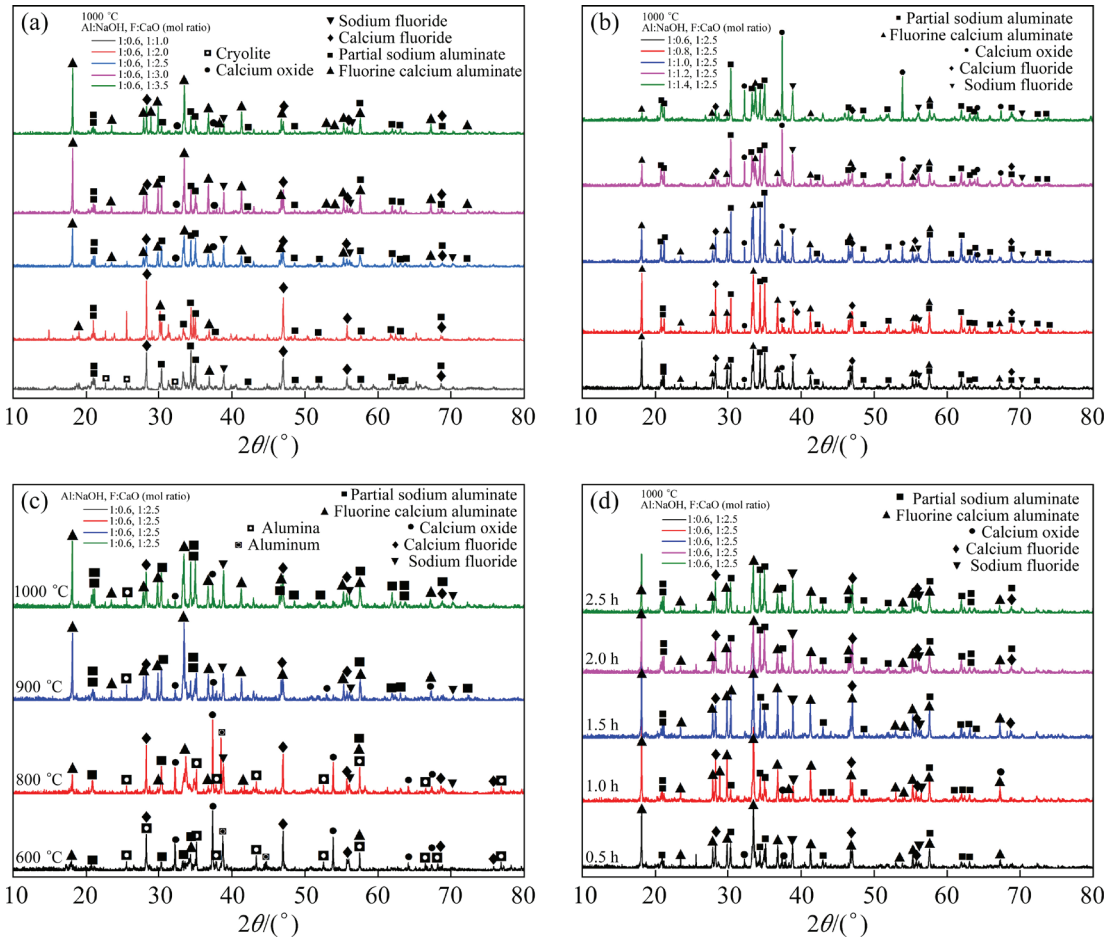

Fig. 6 XRD patterns of roasted samples in different roasting conditions: (a) CaO dosage; (b) NaOH dosage; (c) Roasting temperature; (d) Roasting time

diffraction peaks were basically unchanged, indicating that the reaction reached its optimum state. Therefore, the phase transformation of roasted samples under different conditions could effectively clarify the transformation pattern of aluminum and fluoride in aluminum dross.

3.4 Roasting slag water leaching

The roasting temperature was controlled, and the roasted material did not appear in the molten state. Therefore, it would swell and loosen when exposed to water under agitation. As $NaAlO_2$ has good inter-solubility with water, the roasted material was ground to be less than 74 μm, accounting for 80% of the leached sample. The experiment was carried out at a liquid-to-solid ratio of 10∶1, a water leaching temperature of 60 °C, and a dissolution time of 1.0 h to ensure the effective dissolution of $NaAlO_2$ from the roasted slag. Finally, $NaAlO_2$ was effectively separated from fluoride by filtration and washing to obtain $NaAlO_2$ solution and fluoride residue. The leaching residue was subjected to XRD and SEM−EDS analyses, and the results are shown in Fig. 7. Figure 7(a) shows that the main phases in the leaching slag were CaF_2 and $Ca_{12}Al_{14}F_2O_{32}$, which coincided with the removal of $NaAlO_2$ from the roasting slag. There was no diffraction peak of $NaAlO_2$ appeared in the phase of the leach residue, indicating that $NaAlO_2$ was effectively dissolved during the leaching process. The surface morphology of the leaching slag was investigated by SEM and EDS analyses. Figure 7(b) displays that the white fine particle found by EDS analysis mainly contain O, Ca, Al, and F elements. According to the combination analysis of the XRD results, shaped particles, which contained F and Ca as the main elements, indicated that the area was mainly CaF_2. XRD analysis revealed other spurious peaks, but the peak strength was not high, indicating that the slag contained a small amount of other impurities. Given the good use of fluoroaluminate in quick-setting cements, the residue after water leaching can continue to be of value for its use [40,41].

The aqueous infusion was then crystallized by evaporation and concentrated to obtain a white solid, but it was found to deliquesce easily in air during tests. XRD analysis revealed that this phenomenon was mainly due to the presence of crystalline water in $NaAlO_2$, as shown in Fig. 8(a). To ensure the quality of the product obtained, we thoroughly dewatered the product. Based on the experimental

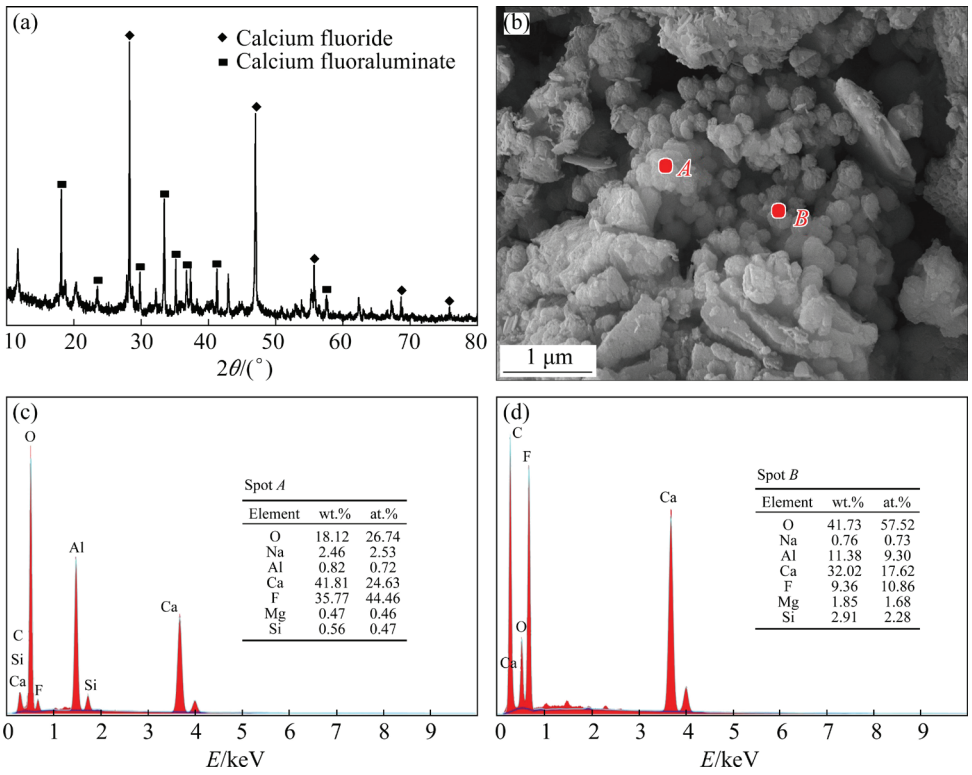

Fig. 7 XRD pattern (a), SEM image (b), and corresponding EDS analysis (c, d) of leached slag, under conditions of 1000 °C, Al to NaOH mole ratio 1∶0.6, F to CaO mole ratio of 1∶2.5, and roasting time 2.0 h

experience, the removal temperature of the majority of substances bound to water was around 200 °C. Therefore, the samples containing crystalline water were placed in a muffle furnace at 200 °C and roasted for dehydration for 2.0 h. After cooling, they were subjected to elemental, XRD, and SEM−EDS analyses, and the results are shown in Table 3, Fig. 8(b), and Fig. 9, respectively. Combined with

Table 3 Comparison of industrial $NaAlO_2$ product quality standard

Category	Sodium oxide content/wt.%	Aluminum oxide content/wt.%	Sodium aluminate content/wt.%	Causticizing coefficient, α_k	Modulus, M	Iron content/wt.%
Industrial indicators	≥30	≥41	≥65	1.15−1.35	0.7−0.8	≤0.002
Experimental indicators	31.32	41.76	67.14	1.23	0.75	−

Causticizing coefficient: mole ratio of Na_2O to Al_2O_3; Modulus: mass ratio of Na_2O to Al_2O_3

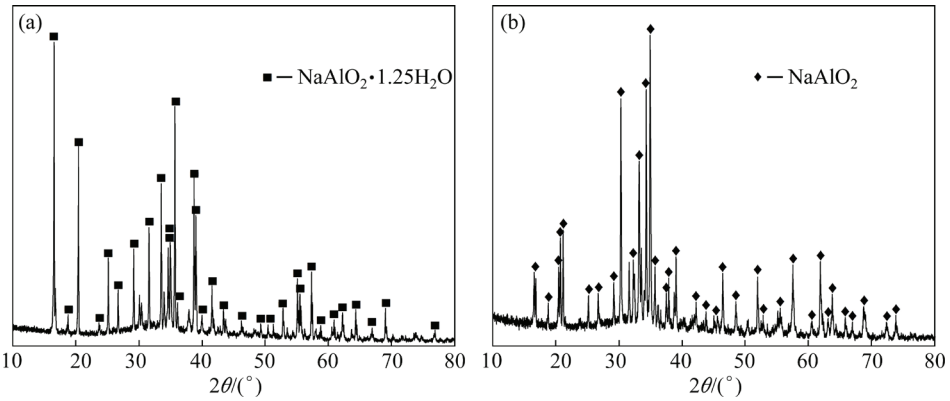

Fig. 8 XRD patterns of evaporation crystallization of water leaching solution (a) and after roasting (b)

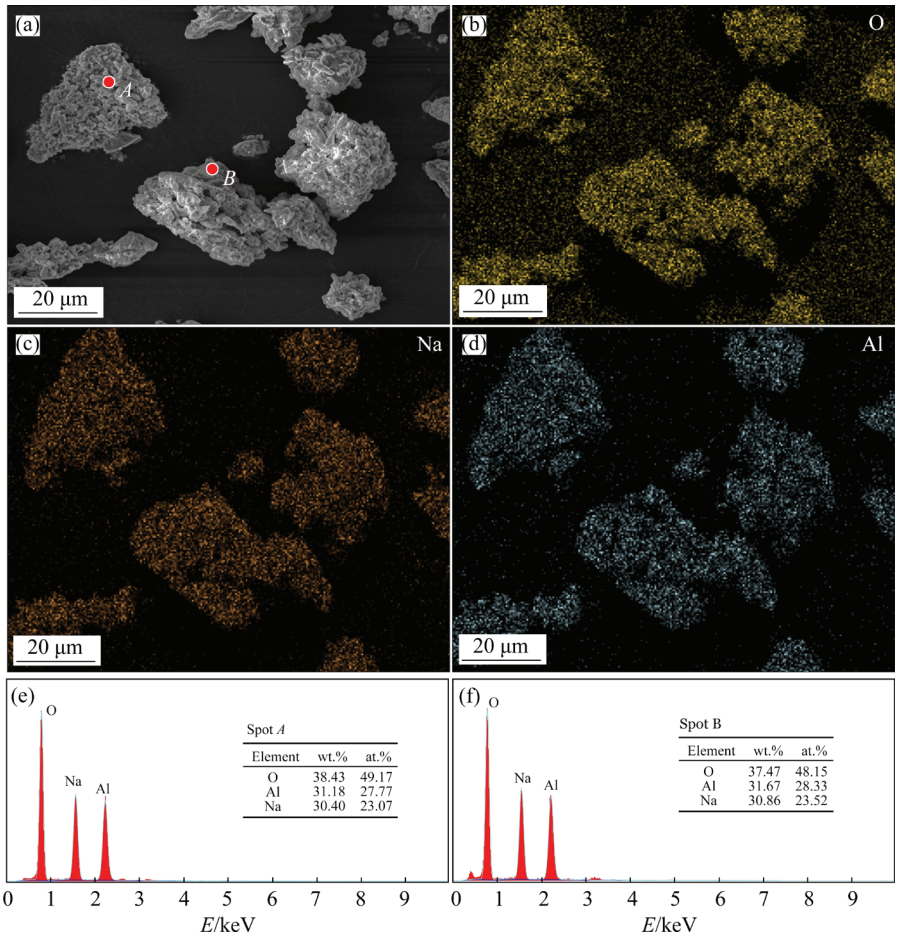

Fig. 9 SEM−EDS analysis of dehydrated products

the different detection methods above, the results showed that the most basic elemental components in the roasting test were Na, Al, and O, which also met the quality requirements of Chinese products ($NaAlO_2$).

4 Conclusions

(1) Under the optimum roasting conditions: roasting temperature of 1000 °C, Al to NaOH mole ratio of 1∶0.6, F to CaO mole ratio of 1∶2.5, and roasting time of 2.0 h, the fluorine solidification rate reached 99.98%, and the aluminum dissolution rate reached 52.97%.

(2) The water leaching solution was crystallized through evaporation, concentrated to obtain $NaAlO_2$ containing crystalline water, and roasted at 200 °C for 2.0 h to obtain the $NaAlO_2$ products, which met the Chinese industrial standard (HG/T 4518−2013).

(3) This study effectively solidified fluoride, but the aluminum utilization rate was low. Subsequent strategies for the effective separation and reuse of Al and F could be explored to fully realize the resourceful recovery of aluminum dross.

CRediT authorship contribution statement

Liang-min DONG: Investigation, Methodology, Data curation, Writing − Original draft; **Fen JIAO** and **Wei LIU:** Project administration, Funding acquisition, Writing – Review; **Ya-lin HUANG** and **Xin WEI:** Investigation, Writing – Review; **Wen-qing QIN:** Supervision, Project administration, Funding acquisition, Writing − Review.

Declaration of competing interest

The authors declare that they have no known competing financial interests or personal relationships that could have appeared to influence the work reported in this paper.

Acknowledgments

The authors gratefully acknowledge the financial support by National Key R&D Program of China (Nos. 2018YFC1902505, 2020YFC1909203), and the National Natural Science Foundation of China (No. 51874356).

References

[1] HOLYWELL G, BREAULT R. An overview of useful methods to treat, recover, or recycle spent potlining [J]. JOM, 2013, 65(11): 1441−1451.

[2] HAVERKAMP R G. An XPS study of the fluorination of carbon anodes in molten $NaF−AlF_3−CaF_2$ [J]. Journal of Materials Science, 2012, 47(3): 1262−1267.

[3] LIAO Chang-zhong, SU Min-hua, MA Sheng-shou, SHIH K, FENG Yong, LIU Cheng-shuai, HO Y K. Immobilization of lead in cathode ray tube funnel glass with beneficial use of red mud for potential application in ceramic industry [J]. ACS Sustainable Chemistry & Engineering, 2018, 6(11): 14213−14220.

[4] ISHAK R, LAROCHE G, LAMONIER J F, ZIEGLER D P, ALAMDARI H. Characterization of carbon anode protected by low boron level: an attempt to understand carbon-boron inhibitor mechanism [J]. ACS Sustainable Chemistry & Engineering, 2017, 5(8): 6700−6706.

[5] TSAKIRIDIS P E. Aluminium salt slag characterization and utilization—A review [J]. Journal of Hazardous Materials, 2012, 217: 1−10.

[6] LI J W, NAKAMURA M, SHIRAI T, MATSUMARU K, ISHIZAKI C, ISHIZAKI K. Mechanism and kinetics of aluminum nitride powder degradation in moist air [J]. Journal of the American Ceramic Society, 2006, 89(3): 937−943.

[7] LIU N W, CHOU M S. Reduction of secondary aluminum dross by a waste pickling liquor containing ferrous chloride [J]. Sustainable Environment Research, 2013, 23(1): 61−67.

[8] International Aluminum Institute. Primary aluminum production [EB/OL]. http://www.world-aluminium.org/statistics/#data.

[9] HONG Jian-ping, WANG Jun, CHEN Hai-yan, SUN Bao-de, LI Jia-jing, CHEN Chong. Process of aluminum dross recycling and life cycle assessment for Al−Si alloys and brown fused alumina [J]. Transactions of Nonferrous Metals Society of China, 2010, 20(11): 2155−2161.

[10] CALDER G V, STARK T D. Aluminum reactions and problems in municipal solid waste landfills [J]. Practice Periodical of Hazardous, Toxic, and Radioactive Waste Management, 2010, 14(4): 258−265.

[11] MESHRAM A, SINGH K K. Recovery of valuable products from hazardous aluminum dross: A review [J]. Resources Conservation and Recycling, 2018, 130: 95−108.

[12] TENORIO J A S, ESPINOSA D C R. Effect of salt/oxide interaction on the process of aluminum recycling [J]. Journal of Light Metals, 2020, 2(2): 89−93.

[13] UEDA M, TSUKAMOTO S, KONDA S, OHTSUKA T. Recovery of aluminum from oxide particles in aluminum dross using $AlF_3−NaF−BaCl_2$ molten salt [J]. Journal of Applied Electrochemistry, 2005, 35(9): 925−930.

[14] GOMEZ E, RANI D A, CHEESEMAN C R, DEEGAN D, WISE M, BOCCACCINI A R. Thermal plasma technology for the treatment of wastes: A critical review [J]. Journal of Hazardous Materials, 2009, 161(2/3): 614−626.

[15] TZONEV T, LUCHEVA B. Recovering aluminum from aluminum dross in a DC electric-arc rotary furnace [J]. JOM, 2007, 59(11): 64−68.

[16] MAJIDI O, SHABESTARI S G, ABOUTALEBI M R. Study of fluxing temperature in molten aluminum refining process [J]. Journal of Materials Processing Technology, 2007, 182(1/2/3): 450−455.

[17] KEVORKIJAN V, ŠKAPIN S D, KOVAČEC U. The nondestructive determination of the aluminum content in pressed skulls of aluminum dross [J]. JOM, 2013, 65(2): 284−293.

[18] SARAVANAKUMAR R, RAMACHANDRAN K, LALY L G, ANANTHAPADMANABHAN P V, YUGESWARAN S. Plasma assisted synthesis of γ-alumina from waste aluminium dross [J]. Waste Management, 2018, 77: 565−575.

[19] ÜNLÜ N, DROUET M G. Comparison of salt-free aluminum dross treatment processes [J]. Resources, Conservation and Recycling, 2002, 36(1): 61−72.

[20] SHINZATO M C, HYPOLITO R. Solid waste from aluminum recycling process: Characterization and reuse of its economically valuable constituents [J]. Waste Management, 2005, 25(1): 37−46.

[21] DASH B, DAS B R, TRIPATHY B C, BHATTACHARYA I N, DAS S C. Acid dissolution of alumina from waste aluminium dross [J]. Hydrometallurgy, 2008, 92(1/2): 48−53.

[22] SARKER M S R, ALAM M Z, QADIR M R, GAFUR M A, MONIRUZZAMAN M. Extraction and characterization of alumina nanopowders from aluminum dross by acid dissolution process [J]. International Journal of Minerals, Metallurgy, and Materials, 2015, 22(4): 429−436.

[23] MAHINROOSTA M, ALLAHVERDI A. Enhanced alumina recovery from secondary aluminum dross for high purity nanostructured γ-alumina powder production: Kinetic study [J]. Journal of Environmental Management, 2018, 212: 278−291.

[24] GHASEMI S M S, AZIZI A. Alkaline leaching of lead and zinc by sodium hydroxide: kinetics modeling [J]. Journal of Materials Research and Technology, 2018, 7(2): 118−125.

[25] TSAKIRIDIS P E, OUSTADAKIS P, AGATZINI-LEONARDOU S. Aluminium recovery during black dross hydrothermal treatment [J]. Journal of Environmental Chemical Engineering, 2013, 1(1/2): 23−32.

[26] JAFARI N H, STARK T E, ROPER R. Classification and reactivity of secondary aluminum production waste [J]. Journal of Hazardous, Toxic, and Radioactive Waste, 2014, 18(4): 4014018.1-11.

[27] ZHANG Yong, GUO Zhao-hui, HAN Zi-yu, XIAO Xi-yuan, PENG Chi. Feasibility of aluminum recovery and $MgAl_2O_4$ spinel synthesis from secondary aluminum dross [J]. International Journal of Minerals Metallurgy and Materials, 2019, 26(3): 309−318.

[28] HASHISHIN T, KODERA Y, YAMAMOTO T, OHYANAGI M, MUNIR Z A. Synthesis of $(Mg,Si)Al_2O_4$ spinel from aluminum dross [J]. Journal of the American Ceramic Society, 2004, 87(3): 496−499.

[29] FOO C T, SALLEH M A M, YING K K, MATORI K A. Mineralogy and thermal expansion study of mullite-based ceramics synthesized from coal fly ash and aluminum dross industrial wastes [J]. Ceramics International, 2019, 45(6): 7488−7494.

[30] CASTRO M N I, ROBLES J M A, HERNÁNDEZ D A C, BOCARDO J C E, TORRES J T. Development of mullite/zirconia composites from a mixture of aluminum dross and zircon [J]. Ceramics International, 2009, 35(2): 921−924.

[31] WAN Bing-bing, LI Wen-fang, SUN Wan-ting, LIU Fang-fang, CHEN Bin, XU Shi-yao, CHEN Wei-ping, YI Ai-hua. Synthesis of cryolite (Na_3AlF_6) from secondary aluminum dross generated in the aluminum recycling process [J]. Materials, 2020, 13(17): E3871.

[32] NIE Yun-fei, GUO Xin-yao, GUO Zhao-hui, TANG Jian-guo, XIAO Xi-yuan, XIN Li-qing. Defluorination of spent pot lining from aluminum electrolysis using acidic iron-containing solution [J]. Hydrometallurgy, 2020, 194: 105319.

[33] DISPINAR D, KVITHYLD A, NORDMARK A. Quality assesment of recycled aluminium [C]//Light Metals. Cham: Springer Interational Publishing, 2011: 731−735.

[34] FENG Hai-gang, ZHANG Guo-fan, YANG Q, XUN Luo-bing, ZHEN Si-yuan, LIU De-zhi. The investigation of optimizing leaching efficiency of Al in secondary aluminum dross via pretreatment operations [J]. Processes, 2020, 8(10): 1269.

[35] ZHANG Yong, GUO Zhao-hu, HAN Zi-yu, XIAO Xi-yuan. Effects of AlN hydrolysis on fractal geometry characteristics of residue from secondary aluminium dross using response surface methodology [J]. Transactions of Nonferrous Metals Society of China, 2018, 28(12): 2574−2581.

[36] XIE Ming-zhuang, GUO Xin-yu, LIU Wei, ZHAO Hong-liang, LI Rong-bin, LIU Feng-qin. Phase transition of waste silicon carbide side block from aluminum smelters during vacuum high-temperature detoxification process [J]. JOM, 2020, 72(7): 2697−2704.

[37] XIE Ming-zhuang, LI Rong-bin, ZHAO Hong-liang, LIU Wei, LU Ting-ting, LIU Feng-qin. Detoxification of spent cathode carbon blocks from aluminum smelters by joint controlling temperature−vacuum process [J]. Journal of Cleaner Production, 2020, 249: 119370.

[38] GUO Hong-wei, WANG Jun, ZHANG Xiu-xia, ZHENG Feng, LI Peng. Study on the extraction of aluminum from aluminum dross using alkali roasting and subsequent synthesis of mesoporous γ-alumina [J]. Metallurgical and Materials Transactions B—Process Metallurgy and Materials Processing Science, 2018, 49(5): 2906−2916.

[39] HU Shao-yan, WANG De-yong, HOU Dong, ZHAO Wei, LI Xiang-long, QU Tian-peng, ZHU Qing-de. Research on the preparation parameters and basic properties of premelted calcium aluminate slag prepared from secondary aluminum dross [J]. Materials, 2021, 14(19): 5855.

[40] BĂDĂNOIU A, PACEAGIU J, VOICU G. Hydration and hardening processes of Portland cements obtained from clinkers mineralized with fluoride and oxides [J]. Journal of Thermal Analysis and Calorimetry, 2011, 103(3): 879−888.

[41] BERTOLINI M J, ZAGHETE M A, GIMENES R, PADOVANI G C. Determination of the properties of an experimental glass polyalkenoate cement prepared from niobium silicate powder containing fluoride [J]. Dental Materials, 2008, 24(1): 124−128.

钙固化碱焙烧−水浸法从二次铝渣中分离氟和铝

董良民[1,2]，焦 芬[1,2]，刘 维[1,2]，黄雅琳[1,2]，魏 鑫[1,2]，覃文庆[1,2]

1. 中南大学 资源加工与生物工程学院，长沙 410083；
2. 中南大学 湖南省战略性含钙矿产资源清洁高效利用重点实验室，长沙 410083

摘 要：设计一种钙固化碱焙烧−水浸出联合工艺处置二次铝渣，研究 CaO 用量、NaOH 用量、焙烧温度和时间对铝溶出和氟固化行为的影响。在最佳实验条件(焙烧温度 1000 ℃、Al 与 NaOH 摩尔比 1∶0.6、F 与 CaO 摩尔比 1∶2.5、焙烧时间 2.0 h)下，氟和铝被分离，其中氟固化率为 99.98%，铝溶出率为 52.97%。水浸液经蒸发结晶，可得到符合中国工业标准的 $NaAlO_2$ 产品；水浸渣可作为速凝水泥原料。总体而言，此研究为处置二次铝渣提供了一个有效、环保的解决方案。

关键词：二次铝渣；钙固化碱焙烧；分离；氟；铝；偏铝酸钠；清洁生产

(Edited by Xiang-qun LI)